PAPER

Investigating the influence of temperature-dependent rheological properties on nanofluid behavior in heat transfer

To cite this article: Mohsan Hassan *et al* 2023 *Nanotechnology* **34** 505404

Nanotechnology **34** (2023) 505404 (13pp) https://doi.org/10.1088/1361-6528/acfb15

Investigating the influence of temperature-dependent rheological properties on nanofluid behavior in heat transfer

Mohsan Hassan[1], **Muhammad Rizwan**[1] **and M M Bhatti**[2,3]

[1] Department of Mathematics, COMSATS University Islamabad, Lahore Campus, 54000, Pakistan
[2] College of Mathematics and Systems Science, Shandong University of Science & Technology, Qingdao 266590, Shandong, People's Republic of China
[3] Material Science Innovation and Modelling (MaSIM) Research Focus Area, North-West University (Mafikeng Campus), Private Bag X2046, Mmabatho 2735, South Africa

E-mail: mmbhatti@sdust.edu.cn and mubashirme@yahoo.com

Received 8 August 2023, revised 13 September 2023
Accepted for publication 18 September 2023
Published 6 October 2023

Abstract

Nanofluids are advanced heat transfer fluids whose performance is influenced by various thermo-physical properties, including nanoparticle volume fraction, base fluid, and temperature. Rheological mathematical models have been established by using empirical data in order to characterize these features as dependent on parameters such as volume fraction, base fluid composition, and temperature. These models have been integrated into transport equations. Nanofluids composed of metallic oxides (Al_2O_3, SiO_2) and carbon nanostructures (PEG-GnP, PEG-TGr) dispersed in deionized H_2O, with nanoparticle concentrations ranging from 0.025% to 0.1%, and temperatures between 30 °C and 50 °C, were utilized to investigate flow over thin needle. The rheological models contained transport equations include the partial differential equations. The transport equations were simplified through various transformations and then solved numerically. The results in form of velocity and temperature distributions were obtained, along with boundary layer parameters, Nusselt number and coefficient of skin friction. The present study contributes to the existing knowledge by elucidating the intricate relationship between nanoparticle volume fraction, base fluid properties, and temperature in nanofluid behavior.

Keywords: heat and mass flow characteristics, rheological modeling, temperature dependent thermophysical, exponential models of viscosity and thermal conductivity

(Some figures may appear in colour only in the online journal)

1. Introduction

Nanofluids, which are fluids containing nanoparticles, are extensively utilized to improve heat transfer in conventional base fluids. These fluids' thermophysical characteristics are improved by the dispersion of metallic or non-metallic nanoparticles. However, the performance of nanofluids is not solely determined by the choice of nanoparticles and base fluid; it also depends on other critical parameters such as nanoparticle shape and size, concentration, clustering, and temperature. These factors are illustrated in figure 1 [1–4].

The thermophysical characteristics of nanofluids, particularly viscosity and thermal conductivity, which rely on temperature and the volume fraction of nanoparticles, have a substantial impact on how well they transport heat. As temperature increases, thermal conductivity improves while viscosity of nanofluids diminishes, according to research that has examined the behavior of viscosity and thermal conductivity in literature. Sundar *et al* [5] investigated the effects of temperature on the viscosity and thermal conductivity of Al_2O_3/H_2O and Al_2O_3/EG nanofluids. The nanofluids were synthesized at 0.3%–1.5% nanoparticle

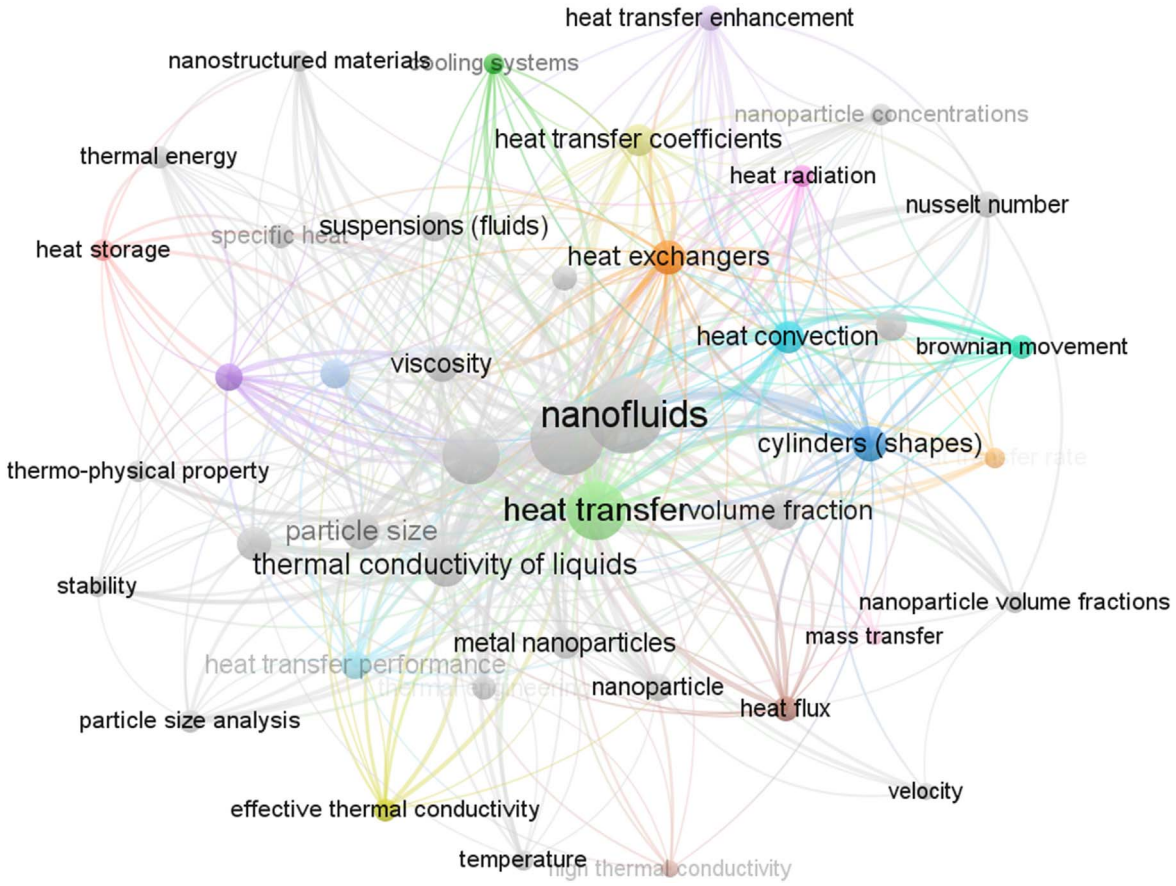

Figure 1. Literature review [1–4] on nanofluid performance factors.

concentrations subjected to variation of temperatures between 25 °C and 60 °C. The findings of the study exposed that as both the temperature and nanoparticle concentration augmented, the thermal conductivity of the nanofluids exhibited an upward trend. Conversely, the viscosity of the nanofluids showed a declining trend with the increase in both temperature and nanoparticle concentration. Moreover, Sundar *et al* [6] examined the same behavior for Fe_3O_4/H_2O nanofluid. The nanoparticle was synthesized at 0%–2% nanoparticle concentration under temperature range 20 °C–60 °C. Furthermore, Gao *et al* [7] analyzed the viscosity and thermal conductivity's behavior for of a Fe_3O_4/H_2O nanofluid under influence of temperature and nanoparticle concentration. The study included the 0.05%–2% nanoparticle concentrations and temperatures changing between 10 °C and 55 °C. Godson *et al* [8] measured the viscosity and thermal conductivity of an Ag/H_2O nanofluid at temperatures ranging from 50 °C to 90 °C and nanoparticle concentrations ranging from 0.3% to 0.9%. Temperature and nanoparticle concentration both increased the thermal conductivity of the nanofluid, according to the findings. On the other hand, viscosity surged with increasing nanoparticle concentration but reduced with increasing temperature. In order to determine their viscosity and thermal conductivity, Xie *et al* [9] studied a number of nanofluids including MgO/EG, SiO_2/EG, TiO_2/EG, Al_2O_3/EG, and ZnO/EG. Temperatures between 10 °C and 60 °C and a concentration of nanoparticles between 0.5% and 5% were utilized in the experiment. The results showed that temperature and nanoparticle concentration both enhanced thermal conductivity and viscosity. The viscosity and thermal conductivity of the nanofluids also showed consistent patterns in a number of investigations looking at the consequences of nanoparticle concentration and temperature [10–15].

Above, it is evident that the viscosity of fluids is significantly influenced by temperature among other factors. Therefore, in heat and mass transfer problems, the impact of temperature on viscosity cannot be overlooked. Typically, temperature-dependent viscosity $\mu(\dot{\gamma}, T)$ is characterized as the product of temperature and shear rate-dependent functions $\mu(\dot{\gamma}, T) = \mu_1(\dot{\gamma})\mu_2(T)$. Here, the shear rate-dependent function is denoted by $\mu_1(\dot{\gamma})$ and the temperature-dependent function by $\mu_2(T)$. Limited viscosity models have been developed in various studies that depend on shear rate and temperature under diverse flow boundary conditions, as highlighted in table 1.

In general, the thermal conductivity of most materials tends to increase as the temperature rises. This can be attributed to the higher energy levels of atoms and molecules within the material, resulting in enhanced thermal transport capabilities. In the literature, different temperature dependent thermal conductivity models are used for different applications as illustrated in table 2.

Table 1. The temperature dependent viscosity models in different studies.

Authors	$\mu_1(\dot{\gamma})$ and $\mu_2(T)$	Remarks
Idowu *et al* [16]	$\mu_1(\dot{\gamma}) = \mu_o$, $\mu_2(T) = a_1 + a_2(T_w - T)$ here T_w is a wall temperature, μ_o is consistency index and a_1 and b_1 are curve fitting parameters	The model demonstrates the linear relationship between temperature and viscosity. It was applied in Casson fluid flow problem over a stretching sheet
Dada *et al* [17]	$\mu_1(\dot{\gamma}) = \mu_o$, $\mu_2(T) = 1 + a_3\left(\frac{T - T_\infty}{T_w - T_\infty}\right)$ here T_∞ is temperature far from surface and a_3 is curve fitting parameter	This model was applied to investigate the flow of non-Newtonian Williamson fluid over a stretching sheet, where viscosity exhibits a linear relationship with temperature
Palani *et al* [18]	$\mu_1(\dot{\gamma}) = \mu_o$, $\mu_2(T) = e^{-a_4 T}$, here a_4 is curve fitting parameter	This model was utilized for Newtonian fluid flow over an isothermal semi-infinite vertical plate where viscosity exhibits a nonlinear behavior with temperature
Kalpana *et al* [19]	$\mu_1(\dot{\gamma}) = \mu_o$, $\mu_2(T) = \frac{1}{a_5(T - T_\infty)}$, here a_5 is curve fitting parameter	The model was used for two-phase boundary layer flow of dusty fluid on plate with nonlinear impact of temperature on viscosity
Hossain *et al* [20]	$\mu_1(\dot{\gamma}) = \mu_\infty$, $\mu_2(T) = \frac{1 + a_3(T - T_\infty)}{T_w - T_\infty}$, here μ_∞ is ambient fluid's viscosity	The model was utilized in convective flow of Newtonian fluid over a vertically isothermal cone
Khan *et al* [21]	$\mu_1(\dot{\gamma}) = \mu_o$, $\mu_2(T) = e^{-a_4(T - T_w)}$	The nonlinear, temperature-dependent viscosity model was applied to study thin film flow over a stretching sheet

Table 2. Temperature dependent thermal conductivity models in different studies.

Authors	Temperature dependent thermal conductivity	Remarks
Idowu *et al* [16]	$k(T) = k_o\{a_1 + b_1(T_w - T)\}$, Here k_o is curve fitting parameter	The model was used in energy equation for Casson fluid on a stretching sheet with linear behavior of temperature on thermal conductivity
Dada, *et al* [17]	$k(T) = k_o\left\{1 + a_3\left(\frac{T - T_\infty}{T_w - T_\infty}\right)\right\}$	The model was employed for heat transport of Williamson fluid flow on the stretching sheet under linear effects of temperature on thermal conductivity
Palani *et al* [18]	$k(T) = k_o(1 + b_3 T)$, Here b_3 is curve fitting parameter	The model was worked for heat equation over an isothermal semi-infinite vertical plate
Kalpana *et al* [19]	$k(T) = \frac{1}{b_4(T - T_w)}$, Here b_4 is curve fitting parameter	The model was used in equation of heat for dusty fluid over a porous media with nonlinear effects of temperature on thermal conductivity
Hossain *et al* [20]	$k(T) = k_o\left\{\frac{1 + b_5(T - T_\infty)}{T_w - T_\infty}\right\}$, Here b_5 is curve fitting parameter	The model was employed in natural heat convection over an isothermal vertical wavy cone where thermal conductivity exhibited linear behavior against temperature
Khan *et al* [21]	$k(T) = k_o\{1 + b_6(T - T_w)\}$, Here b_6 is curve fitting parameter	The model was utilized in energy equation for thin film fluid flow on a stretching sheet where thermal conductivity shows the linear behavior with temperature

Based on the preceding discussion, this article explores the temperature-dependent thermophysical properties of nanofluids, utilizing existing models and experimental observations. The thermophysical characteristics of Al_2O_3/H_2O, SiO_2/H_2O, PEG-GnP/H_2O and PEG-TGr/H_2O nanofluids are specifically examined in this study at a range of nanoparticle concentrations and temperatures, with exponential models developed to match the experimental data. The study is structured into sections, starting with an introduction. Following the introduction, the mathematical models of viscosity and thermal conductivity, along with other properties, are presented. These models are derived through experimental results and served into flow equations for analyzing the flow behavior of schematic nanofluids in section 2. Sections 3 and 4 include the mathematical transport model and physical and boundary layer parameters. The solutions of the transport model are calculated by the RK scheme in section 5. Section 6 gives a brief overview of the graphical results, while section 7 highlights the key findings of the study.

2. Mathematical models for thermophysical properties

In this section, we present mathematical equations that establish correlations for the viscosity, thermal conductivity,

Table 3. The values of curve-fitting parameters of equation (2).

	Al_2O_3		SiO_2		PEG-GnP		PEG-TGr	
$\phi(\%)$	0.025	0.050	0.025	0.050	0.025	0.050	0.0250	0.050
μ_{nf}	0.8388	0.8564	0.8362	0.8457	0.8423	0.8521	0.8349	0.8496
C_1	0.0192	0.0191	0.01931	0.01902	0.0187	0.0184	0.0191	0.0186
n	1.0040	1.0025	1.0076	1.0070	1.0025	1.0024	1.0067	1.0067

Table 4. The results of coefficients ($a_i,\ b_i,\ c_i,\ i = 1,\ 2,\ 3$) of equation (3).

	Al_2O_3			SiO_2			PEG-GnP			PEG-TGr		
	a_i	b_i	c_i	a_i	b_i	c_i	a_i	b_i	c_i	a_i	b_i	c_i
μ_{nf}	0.8	81	−27636	0.8	28	18608	0.8	32	12840	0.8	35	19260
C_1	0.1	−11	0.10	0.1	−18	0.099	0.9	9.9	0.09	0.1	−15	0.10
n	1.0	0	0	1.0	0	0	1.0	0	0	1.0	0	0

Table 5. The results of curve-fitting parameters of equation (4).

	Al_2O_3			SiO_2			PEG-GnP			PEG-TGr		
$\phi(\%)$	0.025	0.050	0.075	0.025	0.050	0.075	0.025	0.050	0.075	0.025	0.050	0.075
$10 \times C_2$	0.049	0.051	0.052	0.044	0.045	0.046	0.058	0.006	0.062	0.058	0.059	0.061
k_{nf}	0.612	0.621	0.628	0.599	0.609	0.617	0.673	0.693	0.712	0.678	0.698	0.718

Table 6. The results of coefficients ($a_i,\ b_i,\ c_i,\ i = 4{,}5$) of equation (5) [23].

	Al_2O_3			SiO_2			PEG-GnP			PEG-TGr		
$\phi(\%)$	a_i	b_i	c_i	a_i	b_i	c_i	a_i	b_i	c_i	a_i	b_i	c_i
$10 \times C_2$	0.23	64	0.238	0.21	40	0.215	.28	80	0.28	0.28	64	0.283
k_{nf}	0.61	27	4920	0.59	35	280	0.64	100	−22 800	0.66	88	−7168

density, and specific heat capacity of nanofluids, utilizing experimental data as a basis. The analysis takes into account four different types of nanofluids, which were synthesized by dispersing Al_2O_3, SiO_2, PEG-GnP, and PEG-TGr in deionized H_2O, respectively, at nanoparticle volume fractions ranging from 0.025% to 0.1%, within a temperature range of 30 °C–50 °C. The data utilized in this analysis was sourced from [22].

2.1. Viscosity

Considering the viscosity model given by equation (1)

$$\mu(T, \dot{\gamma}) = \mu_2(\dot{\gamma})\mu_1(T), \tag{1}$$

where, T is the temperature and $\dot{\gamma}$ is shear rate. The $\mu_1(T)$ is taken in exponential function whereas the $\mu_2(\dot{\gamma})$ is taken in the form of power law model. So, the equation (1) is written as

$$\mu = \mu_{nf}\,|\dot{\gamma}|^{n-1}e^{-(T-T_\infty)C_1}, \tag{2}$$

where, n, μ_{nf} and C_1 are curve-fitting constant. These values are obtained by fitting equation (2) with experimental results [22]. The obtained results in table 3 [23].

Additionally, the aforementioned values are fit into the equation (3), which is denoted as

$$\left.\begin{aligned} \mu_{nf} &= a_1 + c_1\phi^2 + b_1\phi \\ n &= a_2 + c_2\phi^2 + b_2\phi \\ C_1 &= a_3 + c_3\phi^2 + b_3\phi \end{aligned}\right\}, \tag{3}$$

here a_i, b_ic_i, $i = 1, 2, 3$ are coefficients. The curve-fitting coefficients of equation (3) are listed in table 4 [23].

2.2. Thermal conductivity

Given the thermal conductivity model represented by equation (1)

$$k = k_{nf}\,e^{C_2(T-T_\infty)}, \tag{4}$$

where, k_{nf} and C_2 are curve fitting parameters which are obtained by fitting the equation (4) with experimental results [22]. The outcomes of the process of curve fitting are shown in table 5 [23].

Table 7. The values of coefficients of equation (6).

	Al_2O_3		SiO_2		PEG-GnP		PEG-TGr	
	a_6	b_6	a_6	b_6	a_6	b_6	a_6	b_6
ρ_{nf}	1001.5	2000	998.4	2000	991.4	2000	991.5	2000

Table 8. The results of coefficients of equation (7).

	Al_2O_3		SiO_2		PEG-GnP		PEG-TGr	
	a_7	b_7	a_7	b_7	a_7	b_7	a_7	b_7
$(C_p)_{nf}$	3.9945	−19.2	4.10735	−4.52	4.066	−4	4.066	−4

Moreover, the values in table 5 are fitted into following equation

$$\left.\begin{aligned} k_{nf} &= a_4 + b_4\phi + c_4\phi^2 \\ C_2 &= a_5 + b_5\phi + c_5\phi^2 \end{aligned}\right\}, \tag{5}$$

here a_i, $b_i c_i$, $i = 4, 5$ are coefficients and their results are presented in table 6.

2.2.1. Density. The correlation model for density (ρ_{nf}) represented by equation (6) is developed by fitting a first-degree polynomial to the experimental data [22]

$$\rho_{nf} = a_6 + b_6\phi, , \tag{6}$$

where the coefficients a_6 and b_6 of equation (6) obtained from curve fitting are shown in table 7 [23].

2.2.2. Heat capacity. The co-relation model for heat capacity $(C_p)_{nf}$ is developed through curve fitting the polynomial of 1st degree with experimental data [22]. The polynomial for heat capacity is defined as

$$(C_p)_{nf} = a_7 + b_7\phi. \tag{7}$$

The values of equation (7)'s co-efficient a_7 and b_7 are displayed in table 8 [23].

3. Mathematical model for heat and mass flow

Consider a fluid flow over a horizontal, moving thin needle that satisfies the conditions of being irrotational, steady-state, and incompressible within the boundary layer. The velocity of the fluid at the wall of the needle is $u_w(x) = u_1 x^m$ while in the free stream region, it is $u_\infty(x) = u_2 x^m$, where m is velocity index, and u_1 and u_2 are velocities parameters. The temperature of the fluid at the wall of the needle is maintained at a constant value of T_w, and the free stream region is assumed to have a temperature T_∞ ($T_w > T_\infty$). Flow structure over geometry is displayed in figure 2.

In accordance with the boundary layer approximation, the mathematical expressions governing heat and mass transport may be formulated as follows:

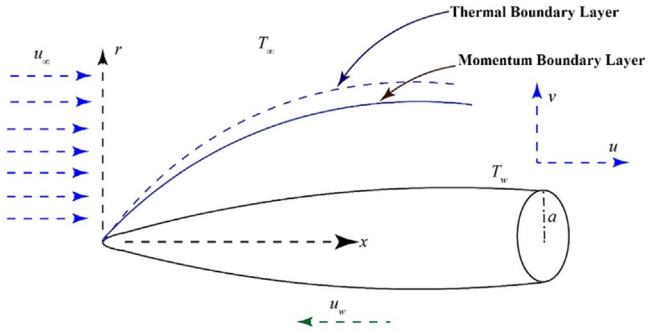

Figure 2. Flow configuration over the needle.

Table 9. The comparison of the values $f''(a)$ with the existing results in [27].

a	Ishak *et al* [27]	Current results
0.1	1.2888	1.28883
0.01	8.4924	8.49238
0.001	62.1637	62.16366

$$\partial_x(ru) + \partial_r(rv) = 0, \tag{8}$$

$$\rho_{nf}(uu_x + u_r v) = \frac{1}{r}\partial_y(\mu r u_r) - p_x \tag{9}$$

$$uT_x + T_r v = \frac{1}{r(\rho C_p)_{nf}}\partial_r(krT_r), \tag{10}$$

where x, r are coordinates axes, u, v are velocity components and T is temperature.

Taking the boundary conditions according to geometry as

$$\left.\begin{aligned} u &= -u_w(x),\ T = T_w v = 0, \text{ at} r = R(x) \\ u &\to u_\infty(x),\ T \to T_\infty \text{as} r \to \infty \end{aligned}\right\}, \tag{11}$$

here $R(x) = \sqrt{\dfrac{a}{A_2 x^{m-1}}}$.

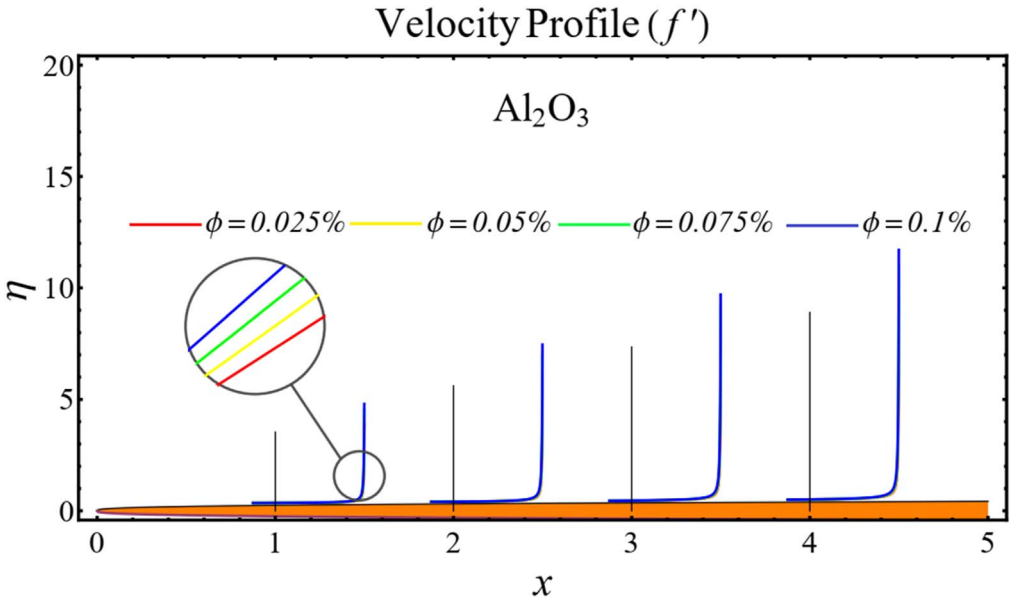

Figure 3. Variations in the velocity profile of Al_2O_3 Nanofluid across differing nanoparticle volume fractions.

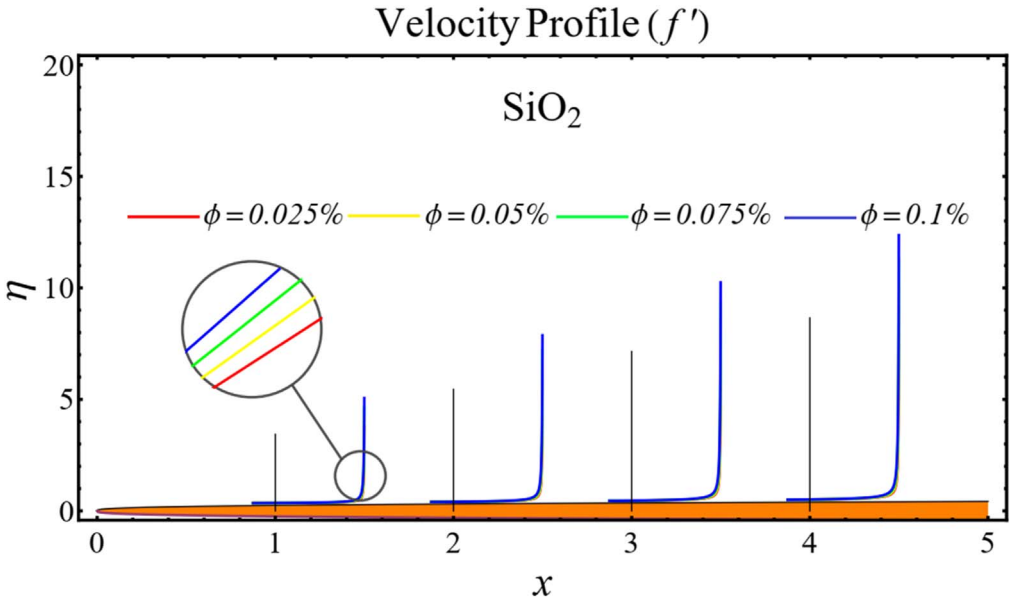

Figure 4. Variations in the velocity profile of SiO_2 nanofluid across differing nanoparticle volume fractions.

To simplify and non-dimensional the above equations, introduced the similarity transformation a.s.

$$\eta = \frac{\mu_{bf}}{\rho_{bf}} u_2 x^{m-1} r^2,\ \psi = \frac{\mu_{bf}}{\rho_{bf}} x f(\eta),$$
$$u = \frac{1}{r}\frac{\partial \psi}{\partial r},\ v = -\frac{1}{r}\frac{\partial \psi}{\partial x} \theta(\eta) = \frac{T - T_\infty}{T_w - T_\infty} \tag{12}$$

After substitution of equation (12) into equations (8)–(11), the following non-dimensional equations are obtained as

$$2\frac{\mu_{nf}}{\mu_{bf}}[f'' + \eta f''' - A\eta f''\theta']e^{-A\theta} + \frac{\rho_{nf}}{\rho_{bf}} \times [ff'' - mf'^2] + \frac{m}{4} = 0, \tag{13}$$

$$2\frac{k_{nf}}{k_{bf}}(\theta' + \eta\theta'' + B\eta(\theta')^2)e^{BT} + \Pr\frac{(\rho C_p)_{nf}}{(\rho C_p)_{bf}} f\theta' = 0, \tag{14}$$

$$\left.\begin{aligned} f(a) = \lambda_1, f'(a) = \lambda_2, \theta(a) = 1, \\ \theta(\infty) = 0, f'(\infty) = \frac{1}{2}, \end{aligned}\right\}, \tag{15}$$

where $A = C_1(T_w - T_\infty)$, $B = C_2(T_w - T_\infty)$, $\lambda_1 = -(m-1)a\lambda_2$, $\lambda_2 = -\frac{1}{2}\frac{u_w(x)}{u_\infty(x)}$, $\mathrm{Re} = \frac{\rho_{bf} u_\infty x}{\mu_{bf}}$ and $\Pr = \frac{\mu_{bf} c_{bf}}{k_{bf}}$.

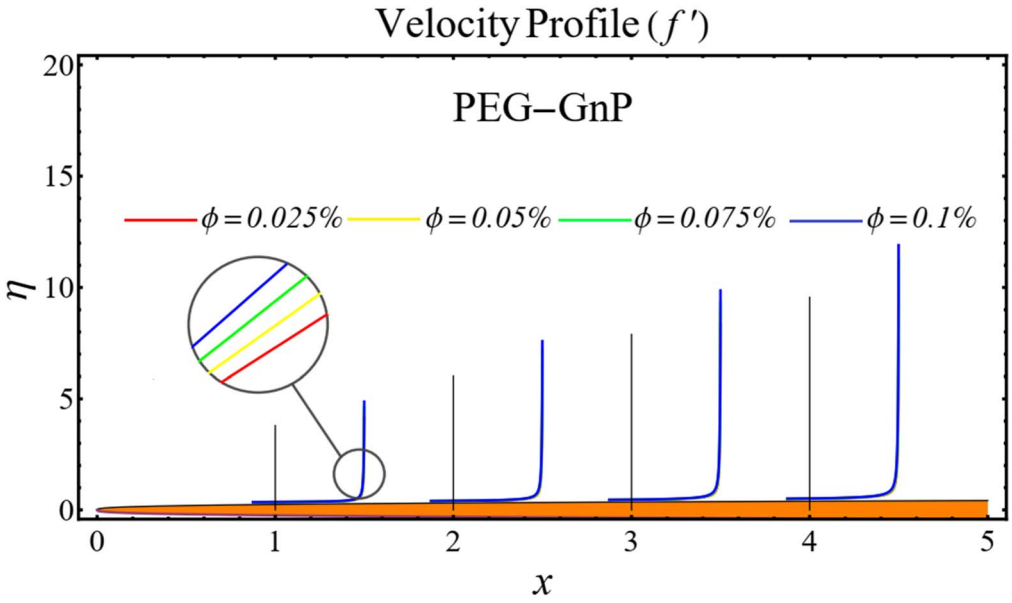

Figure 5. Variations in the velocity profile of PEG-GnP nanofluid across differing nanoparticle volume fractions.

Table 10. The results of temperature dependent parameters A and B at various nanoparticle concentration when $T_w - T_\infty = 20$.

	SiO_2			Al_2O_3			PEG-TGr			PEG-GnP		
$\phi\%$	0.025	0.05	0.075	0.025	0.05	0.075	0.025	0.05	0.075	0.025	0.05	0.075
A	3.873	3.783	3.692	3.865	3.809	3.754	3.817	3.745	3.672	3.749	3.699	3.650
B	0.0982	0.1014	0.1046	0.088	0.09	0.092	0.116	0.12	0.124	0.1162	0.1194	0.1226

4. Physical parameters

4.1. Displacement and momentum thicknesses

The displacement and momentum thicknesses are formulated as

$$\delta^{*2} = \int_{R(x)}^{\infty} r\left(1 - \frac{u}{u_\infty}\right)dr, \tag{16}$$

$$\delta^{**2} = \int_{R(x)}^{\infty} r\frac{u}{u_\infty}\left(1 - \frac{u}{u_\infty}\right)dr \tag{17}$$

After applying the equation (12), the equations (16) and (17) are interpreted as

$$\bar{\delta} = \int_a^{\infty} (1 - 2f')d\eta, \tag{18}$$

$$\bar{\bar{\delta}} = \int_a^{\infty} f'(1 - 2f')d\eta, \tag{19}$$

where $\bar{\delta} = 2A_2\delta^{*2}x^{m-1}$, $\bar{\bar{\delta}} = \delta^{**2}A_2x^{m-1}$.

4.2. Nusselt number and skin friction coefficient

The Nusselt number and coefficient of skin friction are formally defined as

$$C_f = \frac{\tau_w}{\frac{1}{2}\rho_{bf}{u_\infty}^2}, \tag{20}$$

$$Nu_x = \frac{hx}{k_{bf}} \tag{21}$$

In above, τ_w is shear stress and h is represented as convective heat transfer coefficient at wall and expressed as

$$\tau_w = \mu u_r|_{r=R(x)}, \tag{22}$$

$$h = -\frac{k_{nf}\,\partial_r(T - T_\infty)|_{r=R(x)}}{(T_w - T_\infty)}. \tag{23}$$

After applying the transformation equation (12), we get

$$C_f = 8\frac{\mu_{nf}}{\mu_{bf}}a^{\frac{1}{2}}(\mathrm{Re})^{\frac{-1}{2}}f''(a)e^{-A\theta(a)}, \tag{24}$$

$$Nu = -2\frac{k_{nf}}{k_{bf}}a^{\frac{1}{2}}(\mathrm{Re})^{\frac{1}{2}}\theta'(a)e^{B\theta(a)}. \tag{25}$$

5. Solution technique

The solution to equations (13) and (14) in relation to equation (15) is derived by using the Runge–Kutta (RK) scheme. This technique shows promising results as compared with other similar methods [24–26] and it has been widely used. It can be implemented in the following form:

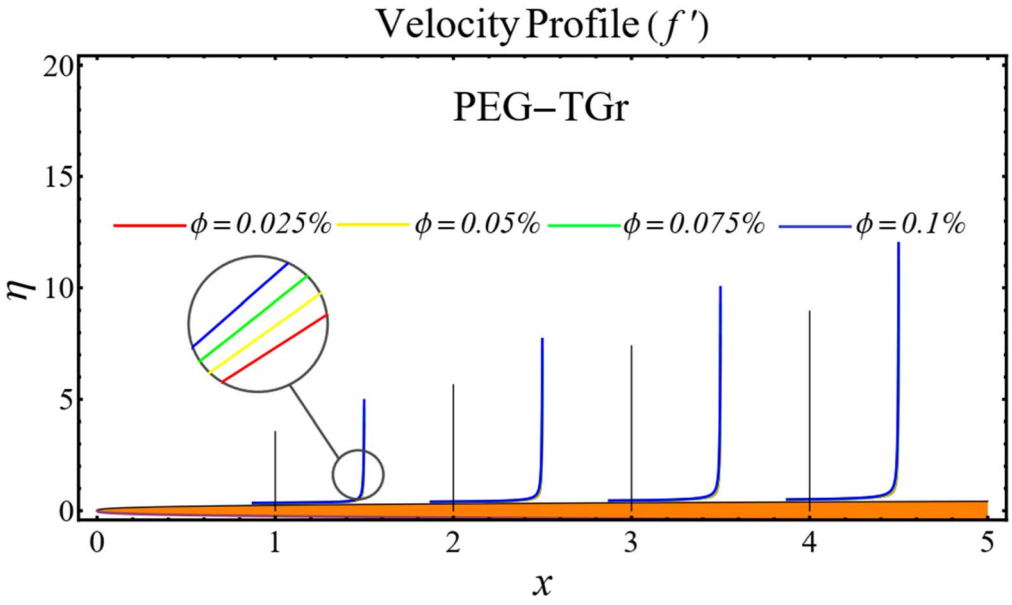

Figure 6. Variations in the velocity profile of PEG-TGr nanofluid across differing nanoparticle volume fractions.

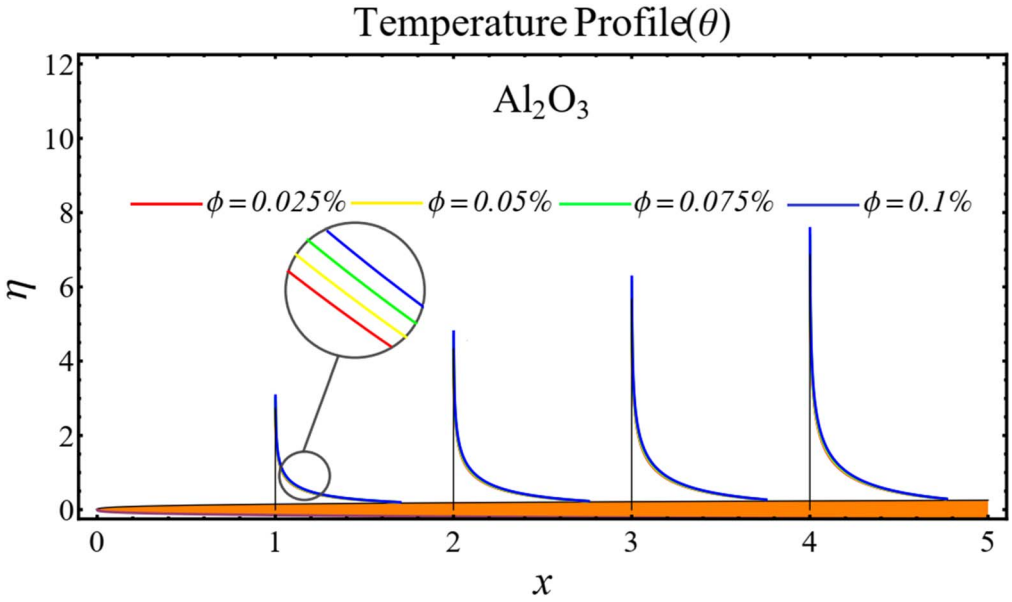

Figure 7. Variations in the temperature profile of Al_2O_3 Nanofluid across differing nanoparticle volume fractions.

Let $f = F_1$, $\theta = G_1$ and convert the equations (13) and (14) into the system of first order differential equations as

$$
\begin{aligned}
&F_1{}' = F_2,\\
&F_2{}' = F_3,\\
&F_3{}' = \frac{1}{\eta}\left[\left(\frac{1}{2}\frac{\rho_{nf}}{\rho_f}\frac{\mu_{bf}}{\mu_{nf}}[mF_2{}^2 - F_1F_3]e^{AG_1} - \frac{m}{4}\right)\right.\\
&\left.-F_3(1 - A\eta G_2)\right],\\
&G_1{}' = G_2,\\
&G_2{}' = -\frac{1}{\eta}\left[\left(\frac{1}{2}\mathrm{Pr}\frac{k_{nf}}{k_f}\frac{(\rho C_p)_{nf}}{(\rho C_p)_{bf}}\left(\frac{m+1}{2}\right)F_1G_2\right)\right.\\
&\left.e^{-BG_1} + G_2(1 + B\eta G_2)\right] \qquad (26)
\end{aligned}
$$

along boundary conditions

$$
\left.\begin{aligned}
&F_1(a) = \lambda_1,\\
&F_2(a) = \lambda_2,\\
&F_3(a) = \Omega_1\\
&G_1(a) = 1\\
&G_2(a) = \Omega_2
\end{aligned}\right\}. \qquad (27)
$$

Here Ω_1 and Ω_2 unknown boundary conditions.

The code was tested by comparing the results with existing data for flow over the same needle geometry, considering limited physical parameters effect existed in the literature. The analysis exposed that the numerical values closely matched the existing data, validating our numerical

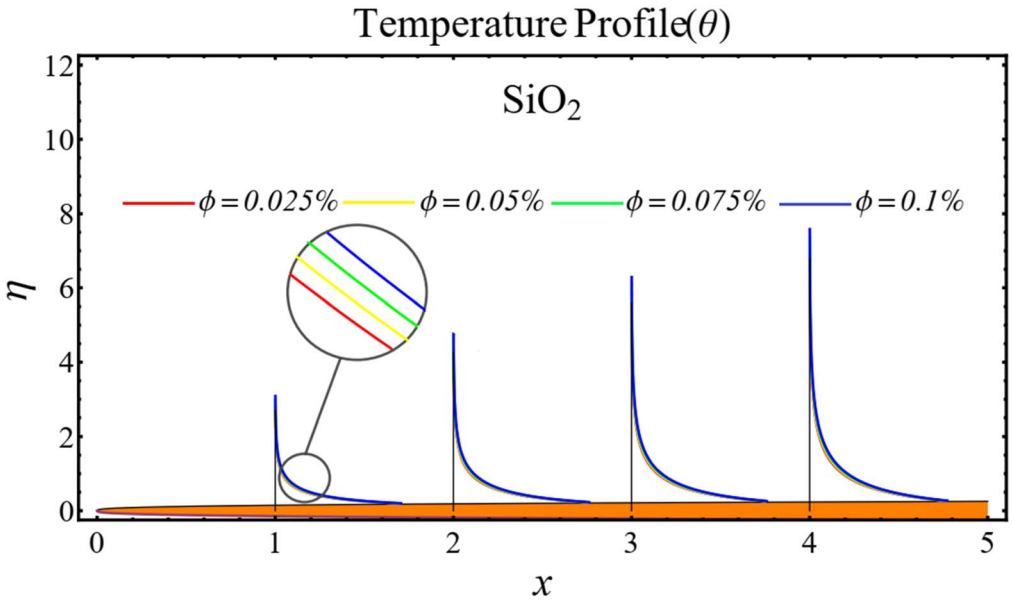

Figure 8. Variations in the temperature profile of SiO2 Nanofluid across differing nanoparticle volume fractions.

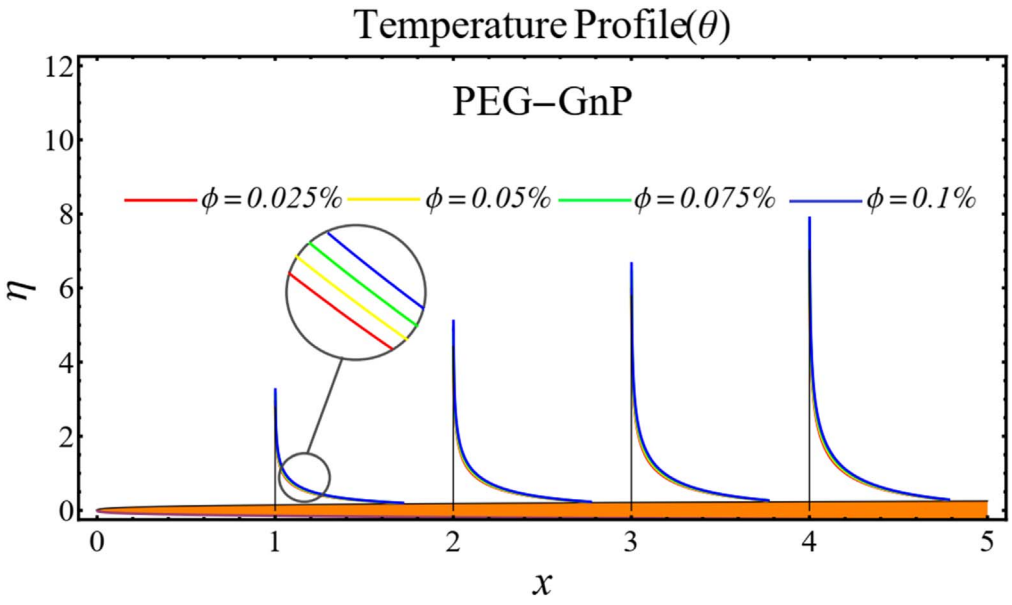

Figure 9. Variations in the temperature profile of PEG-GnP Nanofluid across differing nanoparticle volume fractions.

simulation. The comparison is shown in table 9 when $\phi = 0$ and $\varepsilon = 0$.

6. Results and discussion

The results of velocity and temperature profiles of Al_2O_3/H_2O, SiO_2/H_2O, PEG-GnP/H_2O and PEG-TGr/H_2O nanofluids in graphical form under the impact of various nanoparticle concentration and different temperature for flow over a horizontal thin needle are displayed and discussed. Physical parameters like boundary layers thicknesses, skin friction coefficient and Nusselt number are displayed as well. The results are calculated at fixed values of mainstream and free stream velocities as taken $u_w = 0.01$ and $u_\infty = 0.04$ respectively. Furthermore, the embedding parameters exhibit variability based on the nanoparticle concentration, as shown in table 10.

Figures 3–6 depict the velocity profiles of schematic nanofluids influenced by varying nanoparticle concentrations ranging from 0.025% to 0.075%. The results show that increasing the nanoparticle concentration leads to a reduction in the velocity profiles of the nanofluids. This reduction can be attributed to the increased consistency index resulting from the enhanced nanoparticle concentration. Notably, the effect of nanoparticle concentration on the velocity profile is most significant in the case of the SiO_2/H_2O nanofluid, as it exhibits the largest difference in consistency index values compared to the other nanofluids.

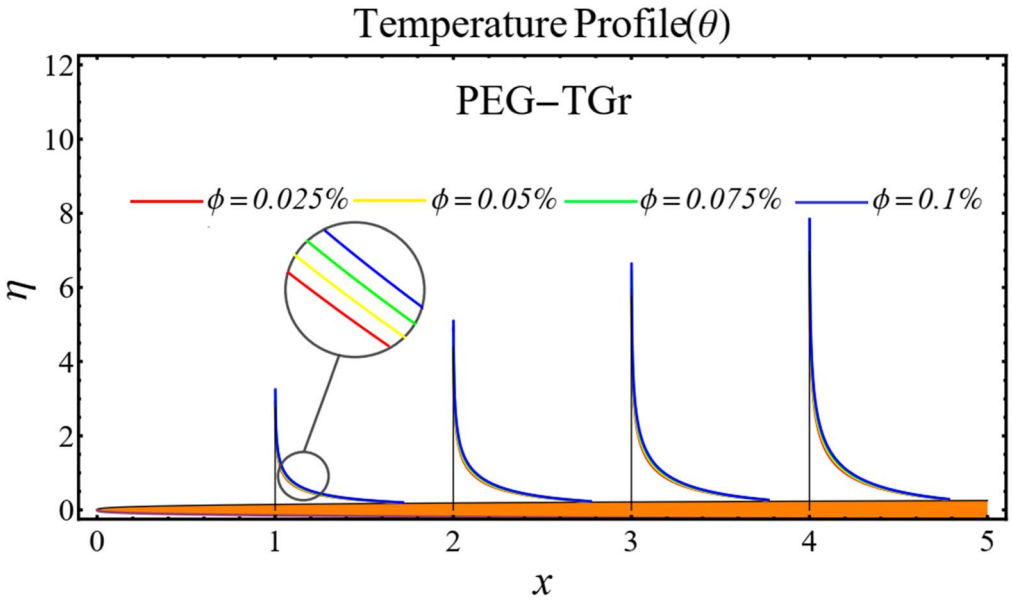

Figure 10. Variations in the temperature profile of PEG-TGr Nanofluid across differing nanoparticle volume fractions.

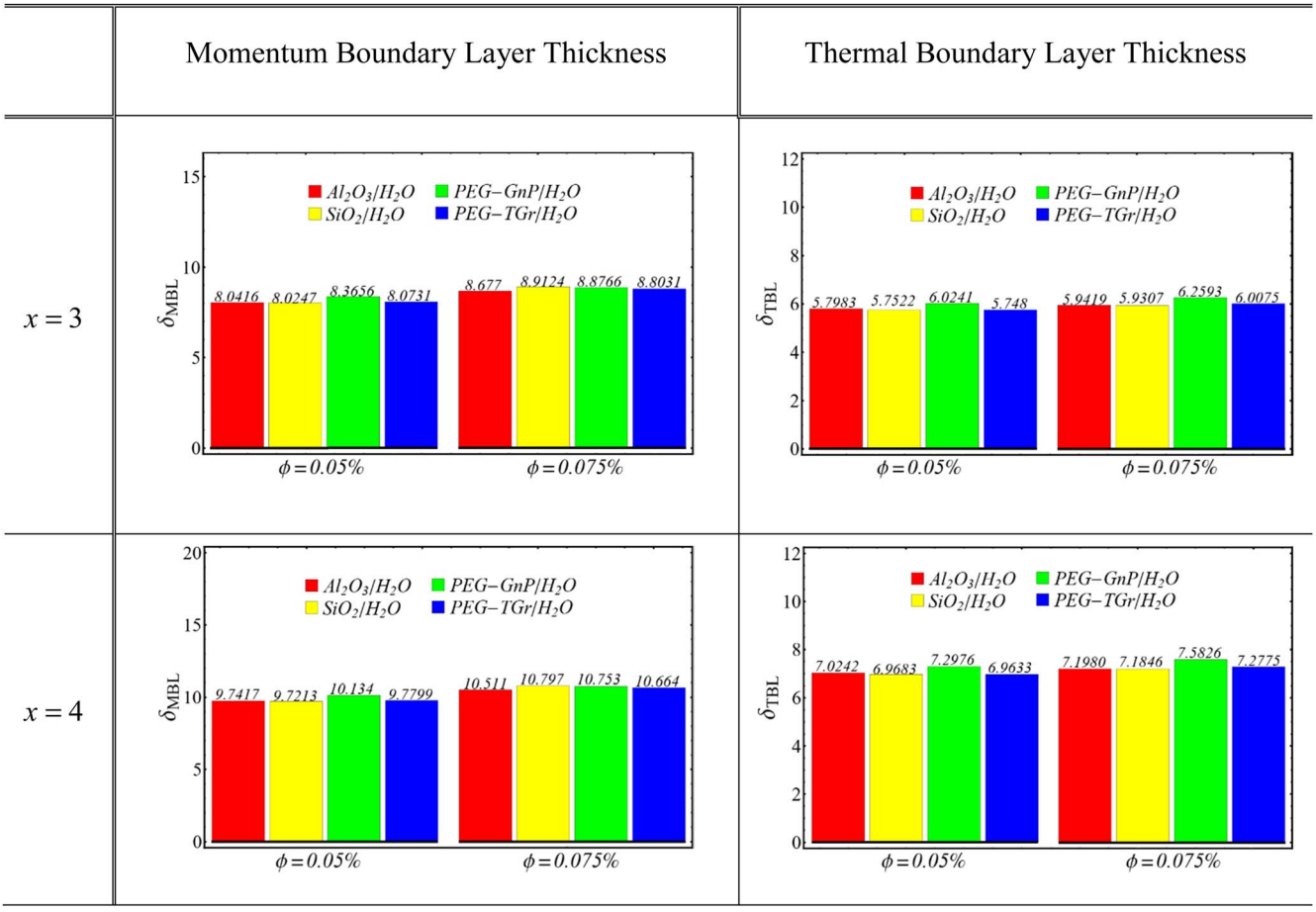

Figure 11. Momentum and thermal boundary layer thickness at various nanoparticle volume fractions and different location on the surface of the needle along x-axis.

Figures 7–10 illustrate the impact of different nanoparticle concentrations on the temperature profiles of schematic nanofluids. The findings indicate that there is a positive correlation between the concentration of nanoparticles and the corresponding temperature profiles of the nanofluids. This behavior is happened due to enhancing thermal conductivity (k_{nf}) and the temperature constant (C_2) as well as the decrease in specific heat resulting from the higher nanoparticle

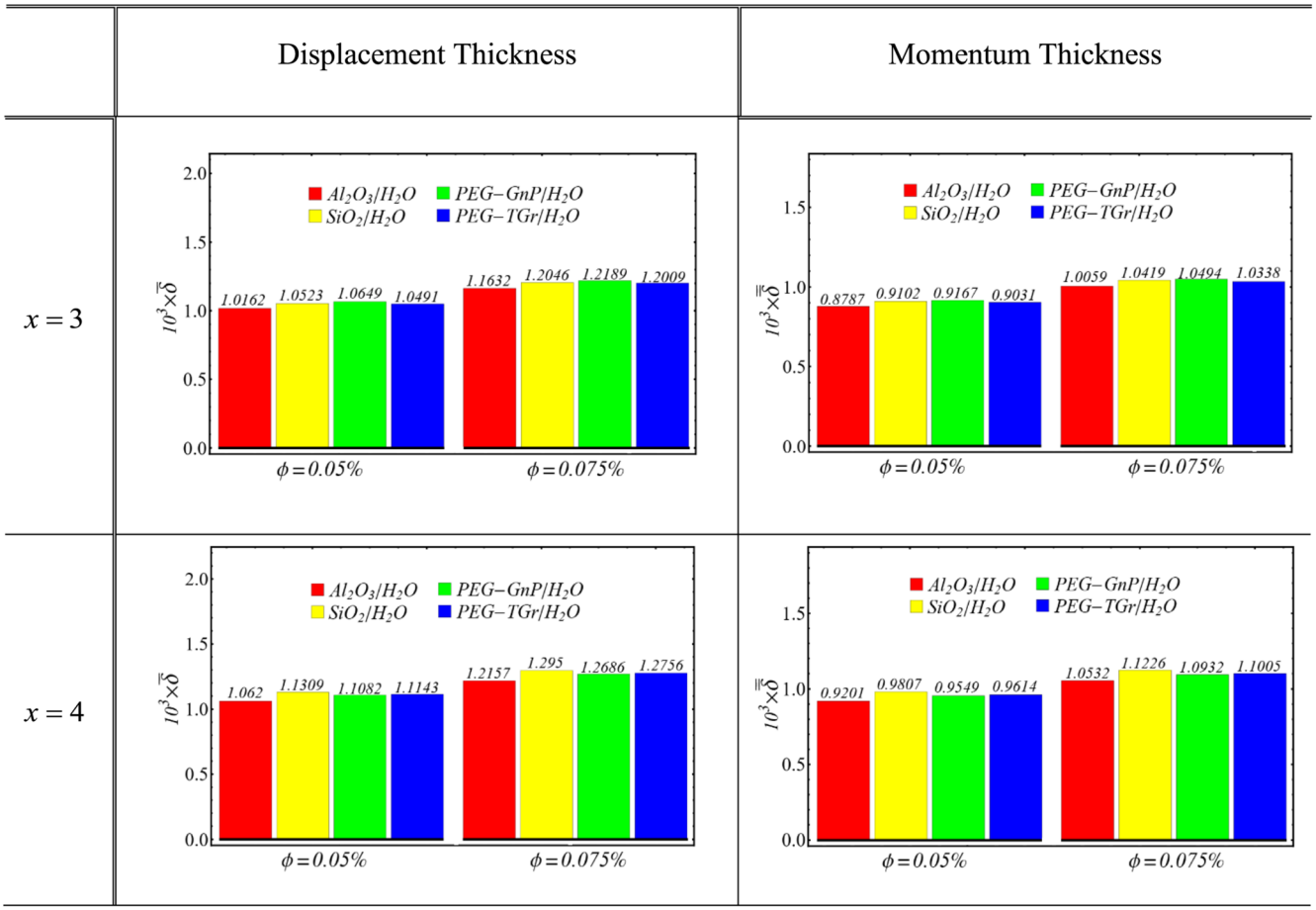

Figure 12. Displacement and momentum thickness at various nanoparticle volume fractions and different location on the surface of the needle along x-axis.

concentration. Notably, when the temperature effect on thermal conductivity becomes zero, the temperature distribution of the fluid slows down. Additionally, the PEG-GnP/H_2O nanofluid exhibits the highest temperature profile due to its superior thermal conductivity compared to other nanofluids.

The graphical representations of velocity profiles, thermal boundary layer thickness, displacement, and momentum thickness for the examined system are shown in figures 11 and 12. In contrast, figure 13 illustrates the outcomes of the skin friction coefficient and Nusselt number.

Figure 11 displays the results of velocity and thermal boundary layer thickness at various locations on x-axis. The findings reveal that both thicknesses increase with higher nanoparticle concentrations, and this enhancement is more prominent along x-axis. The SiO_2/H_2O nanofluid exhibits the maximum thickness values, while the PEG-GnP/H_2O nanofluid shows the minimum thickness values. Furthermore, it has been discovered that the augmentation in nanoparticle concentration results in a subsequent augmentation in both thicknesses, regardless of the influence of operating temperature on the physical attributes.

Figure 12 presents the results of displacement and momentum thickness under the influence of nanoparticle concentration. The displacement thickness increases with higher nanoparticle concentrations, particularly along x-axis. Notably, the PEG-GnP/H_2O nanofluid exhibits the maximum displacement thickness, while the SiO_2/H_2O nanofluid displays the lowest. Similarly, the momentum thickness increases with increasing nanoparticle concentration. Furthermore, both thicknesses show a greater increase when the parameters are considered $C_1 = C_2 = 0$.

Figure 13 presents the coefficient of skin friction and the Nusselt number at various locations on x-axis influenced by nanoparticle concentration. The graphs reveal that the coefficient of skin friction decreases as the nanoparticle concentration increases. This decrease is attributed to the reduced velocity gradient at the wall. Similarly, the Nusselt number values decrease with increasing nanoparticle concentration, resulting from the decreased temperature gradient at the wall. Furthermore, it is observed that the PEG-GnP/H_2O nanofluid exhibits the minimum coefficient of skin friction, while the Al_2O_3/H_2O nanofluid displays the minimum Nusselt number.

7. Conclusions

The current study involves the development of a mathematical model for a homogeneous nanofluid. This model is

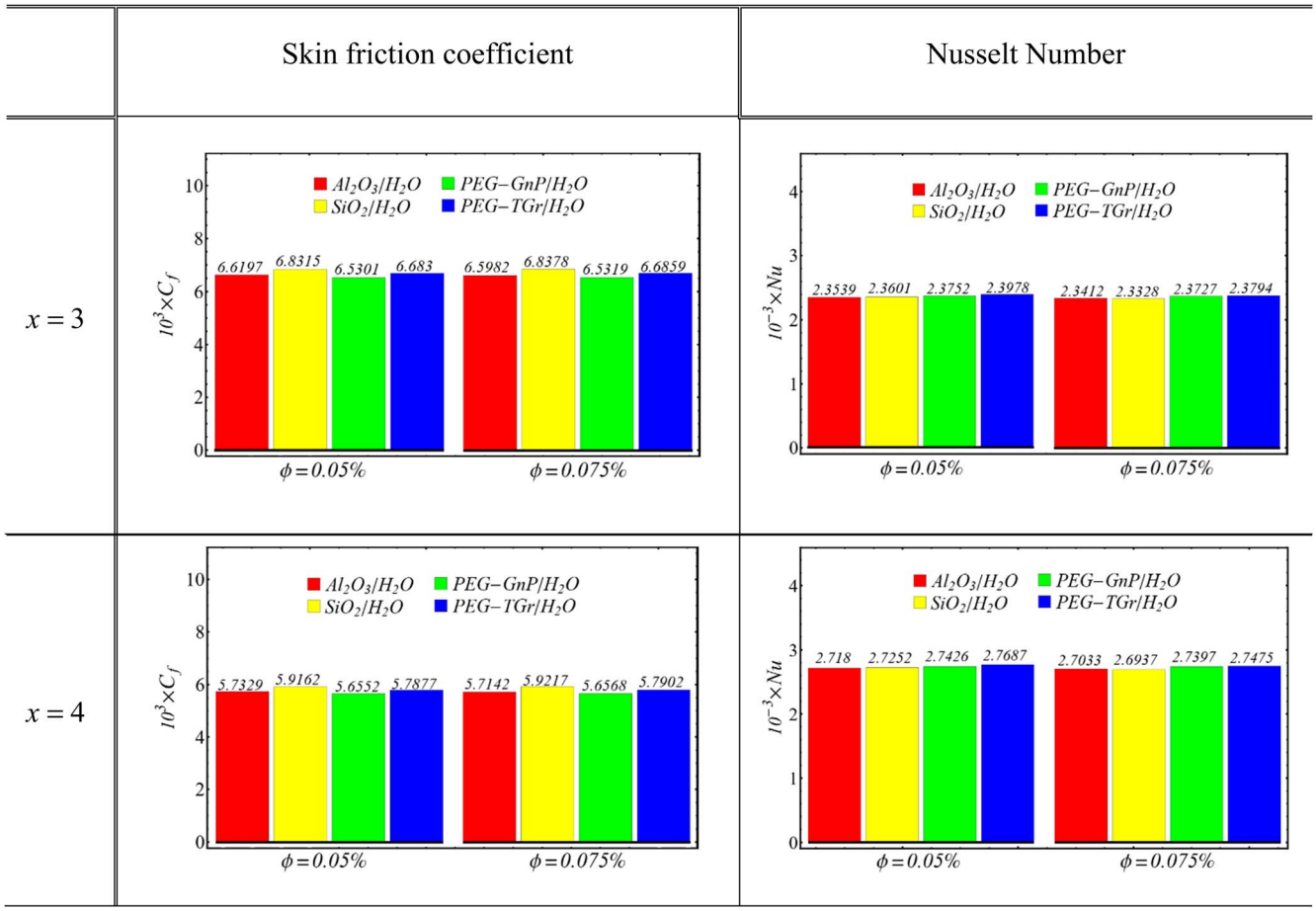

Figure 13. Skin friction coefficient and Nusselt number at nanoparticle volume fractions and different location on the surface of the needle along x-axis.

constructed by using experimental correlations of thermo-physical parameters. The model was used to compute velocity and temperature profiles, thereafter, employed to examine the influence of temperature and nanoparticle concentration on several physical parameters. The results obtained led to the following conclusions:

- As the concentration of nanoparticles in nanofluids rises, there is a corresponding drop in their velocity. Furthermore, this decline is particularly noticeable in cases when the impact of temperature is insignificant.
- In contrast to the velocity profile, the temperature profile exhibits an opposite behavior in response to changes in nanoparticle concentration.
- The boundary layer parameters, including velocity, thermal, displacement, and momentum thicknesses increase with rising nanoparticle concentration. This increase is further amplified when the temperature has no influence.
- The augmentation of nanoparticle concentration results in a drop in both the skin friction coefficient and Nusselt number.

The aforementioned results provide significant contributions to the understanding of nanofluid behavior in relation to changes in nanoparticle concentrations and temperatures.

Data availability statement

The data cannot be made publicly available upon publication because they are not available in a format that is sufficiently accessible or reusable by other researchers. The data that support the findings of this study are available upon reasonable request from the authors.

ORCID iDs

M M Bhatti https://orcid.org/0000-0002-3219-7579

References

[1] Choi S U S and Eastman J A 1995 *Enhancing Thermal Conductivity of Fluids with Nanoparticles* (Argonne National Lab. (ANL)) (No. ANL/MSD/CP-84938; CONF-951135-29)
[2] Eastman J A, Phillpot S R, Choi S U S and Keblinski P 2004 Thermal transport in nanofluids *Annu. Rev. Mater. Res.* **34** 219–46
[3] Tripathi D, Prakash J, Gnaneswara Reddy M and Kumar R 2021 Numerical study of electroosmosis-induced alterations in peristaltic pumping of couple stress hybrid nanofluids through microchannel *Indian J. Phys. Proc. Indian Assoc. Cultiv. Sci. (2004)* **95** 2411–21

[4] Akram J, Akbar N S and Tripathi D 2021 A theoretical investigation on the heat transfer ability of water-based hybrid (Ag–Au) nanofluids and Ag nanofluids flow driven by electroosmotic pumping through a microchannel *Arab. J. Sci. Eng.* **46** 2911–27

[5] Syam Sundar L, Venkata Ramana E, Singh M K and Sousa A C M 2014 Thermal conductivity and viscosity of stabilized ethylene glycol and water mixture Al_2O_3 nanofluids for heat transfer applications: an experimental study *Int. Commun. Heat Mass Transf.* **56** 86–95

[6] Syam Sundar L, Singh M K and Sousa A C M 2013 Investigation of thermal conductivity and viscosity of Fe_3O_4 nanofluid for heat transfer applications *Int. Commun. Heat Mass Transf.* **44** 7–14

[7] Gao D, Bai M, Hu C, Lv J, Wang C and Zhang X 2020 Investigating control of convective heat transfer and flow resistance of Fe_3O_4/deionized water nanofluid in magnetic field in laminar flow *Nanotechnology* **31** 495402

[8] Godson L, Raja B, Lal D M and Wongwises S 2010 Experimental investigation on the thermal conductivity and viscosity of silver-deionized water nanofluid *Exp. Heat Trans.* **23** 317–32

[9] Xie H, Yu W and Chen W 2010 MgO nanofluids: higher thermal conductivity and lower viscosity among ethylene glycol-based nanofluids containing oxide nanoparticles *J. Exp. Nanosci.* **5** 463–72

[10] Nguyen C T, Desgranges F, Roy G, Galanis N, Maré T, Boucher S and Angue Mintsa H 2007 Temperature and particle-size dependent viscosity data for water-based nanofluids—hysteresis phenomenon *Int. J. Heat Fluid Flow* **28** 1492–506

[11] Prakash J, Tripathi D and Anwar Bég O 2023 Computation of EMHD ternary hybrid non-Newtonian nanofluid over a wedge embedded in a darcy-forchheimer porous medium with zeta potential and wall suction/injection effects *Int. J. Ambient Energy* 1–41

[12] Li X, Zou C and Qi A 2016 Experimental study on the thermo-physical properties of car engine coolant (water/ethylene glycol mixture type) based SiC nanofluids *Int. Commun. Heat Mass Transf.* **77** 159–64

[13] Gangadevi R and Vinayagam B K 2019 Experimental determination of thermal conductivity and viscosity of different nanofluids and its effect on a hybrid solar collector *J. Therm. Anal. Calorim.* **136** 199–209

[14] Turgut A, Tavman I, Chirtoc M, Schuchmann H P, Sauter C and Tavman S 2009 Thermal conductivity and viscosity measurements of water-based TiO_2 nanofluids *Int. J. Thermophys.* **30** 1213–26

[15] Bhatti M M, Öztop H F and Ellahi R 2022 Study of the magnetized hybrid nanofluid flow through a flat elastic surface with applications in solar energy *Materials (Basel)* **15** 7507

[16] Idowu A S, Akolade M T, Abubakar J U and Falodun B O 2020 MHD free convective heat and mass transfer flow of dissipative casson fluid with variable viscosity and thermal conductivity effects *J. Taibah Univ. Sci* **14** 851–62

[17] Dada M S and Onwubuoya C 2020 Variable viscosity and thermal conductivity effects on Williamson fluid flow over a slendering stretching sheet *World J. Eng.* **17** 357–71

[18] Palani G and Kim K-Y 2010 Numerical study on a vertical plate with variable viscosity and thermal conductivity *Arch. Appl. Mech.* **80** 711–25

[19] Kalpana G, Madhura K R and Kudenatti R B 2019 Impact of temperature-dependant viscosity and thermal conductivity on MHD boundary layer flow of two-phase dusty fluid through permeable medium *Eng. Sci. Technol. Int. J.* **22** 416–27

[20] Hossain M A, Munir M S and Pop I 2001 Natural convection with variable viscosity and thermal conductivity from a vertical wavy cone *Int. J. Therm. Sci.* **40** 437–43

[21] Khan Y, Wu Q, Faraz N and Yildirim A 2011 The effects of variable viscosity and thermal conductivity on a thin film flow over a shrinking/stretching sheet *Comput. Math. Appl.* **61** 3391–9

[22] Alawi O A, Mallah A R, Kazi S N, Sidik N A C and Najafi G 2019 Thermophysical properties and stability of carbon nanostructures and metallic oxides nanofluids: experimental approach *J. Therm. Anal. Calorim.* **135** 1545–62

[23] Rizwan M, Hassan M, Asjad M I and Tag-ElDin E M 2022 Flow characteristics of heat and mass for nanofluid under different operating temperatures over wedge and plate *Micromachines (Basel)* **13** 2080

[24] Abo-Dahab S M, Abouelregal A E and Marin M 2020 Generalized thermoelastic functionally graded on a thin slim strip non-Gaussian laser beam *Symmetry (Basel)* **12** 1094

[25] Othman M I A, Fekry M and Marin M 2020 Plane waves in generalized magneto-thermo-viscoelastic medium with voids under the effect of initial stress and laser pulse heating *Struct. Eng. Mech.* **73** 621–9

[26] Bhatti M M and Ellahi R 2023 Numerical investigation of non-Darcian nanofluid flow across a stretchy elastic medium with velocity and thermal slips *Numer. Heat Transf.*B **83** 323–43

[27] Ishak A, Nazar R and Pop I 2007 Boundary layer flow over a continuously moving thin needle in a parallel free stream *Chin. Phys. Lett.* **24** 2895–7